Chemical and Biological Technologies in Agriculture

RESEARCH

Open Access

Evaluation of anti-aging and antioxidant properties of a new rose variety, *Ever-rose*

Se Jik Han[1†], Polina Belousova[1†], Sangwoo Kwon[2†], Jihui Jang[3], Jun Bae Lee[3], Hyunjae Kim[4], Gayeon You[5], Jihyeon Song[5], Hyejung Mok[5], Ho Su Ha[6], So Jeong Bae[6], In Jin Ha[7], Min Young Lee[7] and Kyung Sook Kim[1,2*]

Abstract

Background Rose flowers contain active ingredients such as flavonoids and volatile oils and are acknowledged to be good natural resources owing to their anti-aging and antioxidant properties. In this study, we develop four new rose varieties (named *Ever-rose*) that are fragrant, pest resistant, and easy to grow. Subsequently, we evaluate the properties of *Ever-rose* and its potential for use in anti-aging products.

Methods The chemical composition of *Ever-rose* was determined using ultra-high-performance liquid chromatography triple time-of-flight mass spectrometry/mass spectrometry. The antioxidant activity of the *Ever-rose* extract was evaluated using various assays, including superoxide dismutase activity, 2,2-diphenyl-1-picrylhydrazyl radical-scavenging capacity, and xanthine oxidase activity. The variations in proteolytic matrix metalloproteinase-1 expression, collagen content after ultraviolet (UV) irradiation, and reactive-oxygen-species (ROS) levels after infrared A (IRA) treatment were evaluated. The variations in cell elasticity were assessed via atomic force microscopy.

Results The petal extracts of *Ever-rose* (named ER004(P), ER011(P), ER012(P), and ER015(P)) showed good antioxidant activity. They effectively inhibited UV irradiation-induced MMP-1 expression and IRA irradiation-induced increase in mitochondrial ROS levels. Additionally, they inhibited variations in cell shape and elasticity as aging progressed. In particular, ER011(P) demonstrated the best anti-aging and antioxidant effects.

Conclusion The newly developed *Ever-rose* showed excellent antioxidant and anti-aging effects. In particular, ER011(P) demonstrated the best properties owing to its high antioxidant content. Hence, it exhibits significant potential as a functional cosmetic ingredient.

Keywords Anti-aging, Antioxidant, Rose extracts, Cellular elasticity, Atomic force microscopy (AFM)

†Se Jik Han, Polina Belousova, and Sangwoo Kwon have contributed equally to this work.

*Correspondence:
Kyung Sook Kim
moosou94@khu.ac.kr
Full list of author information is available at the end of the article

Graphical Abstract

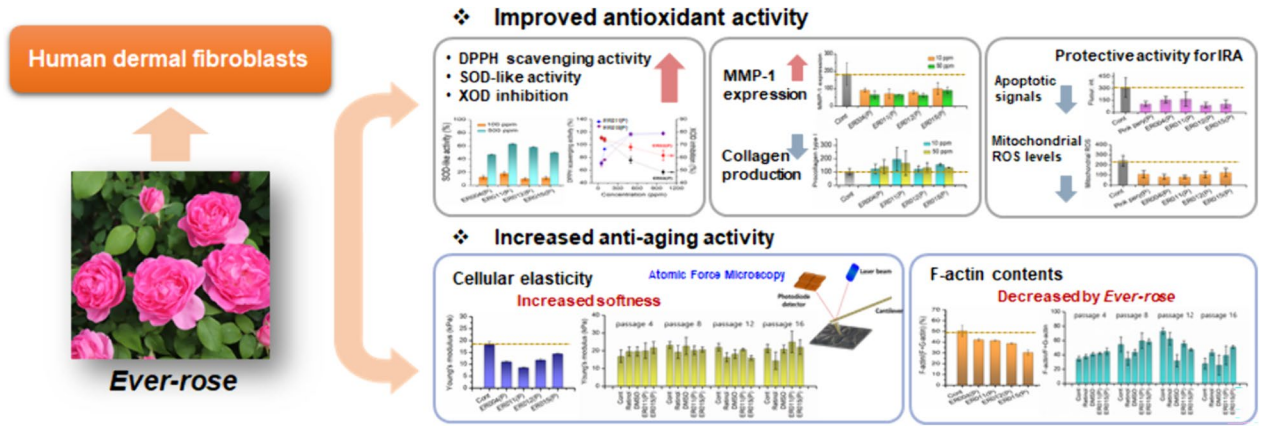

Background

Intrinsic skin aging, which is a chronological process that occurs naturally over time, is induced or exacerbated by external stress. Various external stressors including sunlight, atmospheric pollutants, and extreme temperatures are involved in skin aging. Aging skin is characterized by wrinkles, elasticity loss, sagging, and rough texture [1], which are caused by phenotypic transformations in cells (e.g., fibroblasts and melanocytes) as well as structural and functional variations in extracellular matrix (ECM) components such as collagen, elastin, and proteoglycans [2].

The content and function of ECM proteins in the skin are altered by aging dermal fibroblasts and external stressors, particularly ultraviolet B (UVB) [3]. UV irradiation increases intracellular reactive oxygen species (ROS) levels, thus resulting in oxidative stress and hence ECM remodeling [4]. Oxidative stress promotes the expression of proteolytic matrix metalloproteinases (MMPs), which reduces collagen synthesis and accelerates collagen degradation. Many studies have demonstrated that antioxidants can improve cell function, increase collagen production, improve elasticity, generate younger cells, and reduce UV damage [5]. Antioxidants function as scavengers of free radicals and are primarily observed in seeds, fruits, flowers, and leaves. The most potent antioxidants are phenolic and polyphenolic compounds, flavonoids, phytic-acid substances, and nitrogenous compounds [6].

The rose is a perennial flowering plant belonging to the *Rosaceae* family. It has been used as a skincare ingredient since ancient times and remains widely used in various skincare products [7]. Rose petals contain various phenolic compounds, phenolic acids, and phenolic phytochemicals such as polyphenols, tannins, flavonoids, phenolic acids, and anthocyanins [8–10]. These components are rich in vitamins, essential fatty acids, and minerals, as well as exhibit anti-inflammatory and antibacterial properties [11]. Therefore, roses are remarkable natural antioxidants that can strengthen skin cells and regenerate skin tissue.

Over 150 varieties of roses are widely used in cosmetics and medicine [12]. A widely used *Rosa* species is *Rosa damascena*, similarly known as *Damask rose*, which is native to the Middle East and Central Asia [10]. It exhibits strong anti-aging and antibacterial properties, which renders it effective for soothing irritating skin and healing wounds [13–15]. Another common variety used in cosmetics is *Rosa centifolia* (generally known as cabbage roses). It is rich in vitamin C and tannins, thus providing toning and antioxidant advantages [16]. However, black, baby, French, and alpine roses are less commonly used in cosmetics [17].

Through cross-breeding, we developed four new varieties of roses (ER004, ER011, ER012, and ER015) with excellent disease resistance and growing characteristics, which we named *Ever-rose*. These varieties were developed for use as garden roses and feature strong, long-lasting fragrances as well as excellent characteristics such as disease resistance, drought tolerance, cold hardiness, growth vigor, continuous blooming, and multi-flowering. In this study, the chemical compositions of four types of *Ever-rose* were identified, and the antioxidant and anti-aging properties of freeze-dried extracts of their rose petals and leaves were evaluated. Based on the results, we determined the *Ever-rose* variety that is the most suitable as an antioxidant or anti-aging agent.

Materials and methods

Development of new garden-rose variety (*Ever-rose*)

To develop garden roses with strong fragrances and desirable traits such as disease resistance, we obtained various rose breeds, including fragrant roses from our existing rose gardens, David Austin roses, and roses from the Knock Out series renowned for their disease resistance. More information on the development of new garden rose varieties can be found in the supplementary material (Method S1).

Ever-rose variety cultivation

Ever-rose has been propagated using cutting methods. Cuttings allow for year-round production in greenhouses and can prevent soil-borne diseases transmissible from the soil. Additionally, after rooting the cuttings, they can be transferred easily to pots. The detailed process of cutting and growing is as follows:

(1) Cutting

After the flowers have bloomed, the branches were cut into segments comprising two nodes each using pruning shears disinfected with 70% alcohol. The cuttings were dipped in a 1,000 × diluted solution of sodium hypochlorite and then inserted into a growing medium without fertilizer, with the rooting segment facing downward. The roots should develop within approximately 30 days. During this period, the cutting was sprayed with Benomyl solution at 1000 × dilution once a week for disinfection.

(2) First transplant

The rooted roses were transplanted into pots. A growing medium that containing trace nutrients was used. Sufficient moisture retention by the medium was ensured by watering for an extended period. The medium used was a mix comprising perlite and peat moss.

(3) Second transplant

Once the roses have grown to a certain size, they were re-transplanted into growth pots and allowed to be grown indoors. Around June, the plants were transferred outdoors to grow for 6–7 months.

Ever-rose extracts

The *Ever-rose* used in this study were grown in Everland (Gyeonggi-do, Republic of Korea). As a preliminary experiment, the whole plant, petals, leaves, and stems were dried and extracted separately. Because the petals and leaves exhibited efficient drying and high extraction yields, we performed the next experiment on them. The dry yields of the petals and leaves were 13.1–18.2% and 23.4–30.1%, respectively. The petals were harvested at full bloom, whereas the leaves were harvested at the non-defoliated leaf stage for use in the experiment. The petals and leaves were washed and dried in an oven at 60 °C for 10 h. Their extracts were obtained by treating 100 g of dried petals and leaves each with 30% ethanol at 60 °C for 5 h. Subsequently, the extracts filtered separately and concentrated under reduced pressure using a rotary evaporator. The concentrated solution was dried under reduced pressure at 80 °C to prepare the extract powder.

Chemical profiles of extracts from four *Rosa* species using ultra-high-performance liquid chromatography triple time-of-flight mass spectrometry/mass spectrometry (UHPLC-triple TOF–MS/MS)

A chromatographic analysis of the rose extract was performed using UHPLC-triple TOF–MS/MS to identify the chemical components of the rose. Approximately 50 mg of rose extract was agitated with 1 mL of 50% ethanol using a vortex mixer for 30 s and then sonicated for 10 min. The supernatants were filtered through a 0.2 μm hydrophilic polytetrafluoroethylene syringe filter (Thermo Fisher Scientific, Sunnyvale, CA, USA). Finally, the filtrate was diluted in a four-fold diluted concentration and transferred to a liquid chromatography (LC) vial before use. The LC–MS system comprised a Thermo Scientific Vanquish UHPLC system (Thermo Fisher Scientific) with a Kinetex EVO C18 column (2.1 mm × 100 mm, 1.7 μm) coupled to a Triple TOF5600$^+$ mass spectrometer system (QTOF MS/MS, SCIEX, Foster City, CA, USA). The QTOF MS was equipped with an electro-spray ionization source in positive and negative ion modes and was used to complete the high-resolution experiment. The elution program for UHPLC separation using 0.1% formic acid in water as eluent A and 0.1% formic acid in acetonitrile as eluent B was as follows: 0–1 min, 5% B; 1–4 min, 5–15% B; 4–7 min, 15–20% B; 7–9 min, 20% B; 9–12 min, 20–30% B; 12–14 min, 30–35% B; 14–18 min, 35–50% B; 18–23 min, 50–100% B; 23–28 min, 100% B and equilibration with 5% B for 4 min at a flow rate of 0.4 mL/min. The column temperature was 40 °C and the auto-sampler was maintained at 4 °C. The injection volume of each sample solution was 2 μL. Data acquisition and processing for qualitative analysis were performed using Analyst TF 1.7, PeakVeiw2.2 and MasterView (SCIEX, Foster City, CA, USA).

Cell culture

Human dermal fibroblasts (HDFs) purchased from Thermo Fisher Scientific (Waltham, MA). were grown in Dulbecco's modified Eagle medium (DMEM; Thermo Fisher Scientific) with high glucose supplemented with 10% fetal bovine serum (FBS; Thermo Fisher Science) and 0.1% gentamicin (Thermo Fisher Scientific). They were

seeded at a density of 1×10^5 cells/well and subsequently incubated at 37 °C and 5% CO_2. The cells were cultured for up to 16 passages for cell senescence.

Cell viability

The effects of the *Ever-rose* extract on cell viability were analyzed using a 3-(4,5-dimethylthiazol-2-yl)-2,5-diphenyl tetrazolium bromide (Sigma-Aldrich, St. Louis, MO, USA) assay. HFDs were seeded into culture dishes (diameter = 35 mm) at a density of 4.5×10^5 cells/well and treated with petal and leaf extracts for 24 h. EZ-Cytox solution (DoGen Bio, Seoul, Korea) was added to each cell dish (10 mL) and incubated at 37 °C for 1 h. A Multiskan EX ELISA microplate reader (Thermo Fisher Scientific) was used to measure the absorbance at 450 nm.

MMP-1 inhibitory activity

HDFs were seeded in 24-well plates at 1.0×10^5 cells/well with *Ever-rose* extract and allowed to stabilize for 24 h. For UVB irradiation, the existing medium was removed and the cells washed with phosphate-buffered saline (PBS). Subsequently, the cells were exposed to UVB (22.5 mJ/cm^2) using an ultraviolet P (UVP) crosslinker (Analytik Jena AG, Jena, Germany). Next, the cells were incubated for 24 h in a medium supplemented with petal and leaf extracts. Subsequently, they were cultured in an FBS-free medium supplemented with petal and leaf extracts for 24 h. The extent of MMP-1 secretion in the medium supernatant was measured using an MMP-1 human ELISA kit (ab100603, Abcam, USA). Briefly, standard solutions or samples were added to each well and incubated at room temperature. The prepared biotin antibody, streptavidin solution, TMB one-step development solution, and STOP Solution were added to each well. The color intensity was measured at 450 nm.

Procollagen type I

To measure the procollagen type-I synthesis activity of the *Ever-rose* extract, the cells were seeded in 24-well plates at 1.0×10^5 cells/well and stabilized for 24 h. The medium in the plates was removed, and the cells were cultured in FBS-free medium supplemented with petal and leaf extracts for 24 h. The procollagen type-I secretion in the supernatant was measured using a procollagen type-I C-peptide (PIP) EIA kit (MK101, Takara, Japan). Briefly, we prepared the reagents, samples, and standards as instructed, added 50 µL of the sample to 24-well plates, added 50 µL of antibody cocktail to all the wells, incubated the assembly at room temperature for 1 h, washed each well thrice with 350 µL 1X wash buffer, added 100 µL TMB development solution to each well, incubated the assembly 10 min, added 100 µL of STOP solution, and then read the OD at 450 nm.

Superoxide dismutase (SOD) activity

The SOD activity was measured using an SOD determination kit (Sigma, MO, USA). The rose extract was diluted to the appropriate concentration, and 20 µL aliquots were dispensed into a 96-well plate. Additionally, WST solution (200 µL) and enzyme reaction solution (20 µL) were added to the well plate. After incubation at 37 °C for 20 min, the absorbance was measured at 450 nm using a microplate reader (BioTek, VT, USA). The SOD activity was calculated as follows [18]:

$$\text{SOD enzyme activity (\%)} = \frac{1 - (A_T - A_S)}{(A_C - A_B) \times 100}, \quad (1)$$

where A_T, A_S, A_C, and A_B denote the absorbance of the test group, *Ever-rose* extract, control group, and blank, respectively. The test group comprised an enzyme working solution and the rose extract.

Xanthine oxidase (XOD) activity

The XOD inhibitory activity was analyzed using an XOD assay kit (AAT Bioquest, Sunnyvale, CA, USA). Sample solutions were prepared using the *Ever-rose* extract at concentrations ranging from 50 to 1,000 ppm. XOD (50 µL) was added to the sample solution. The mixture was incubated for 30–60 min at 37 °C. Subsequently, the solution absorbance was measured at 570/610 nm using an ELISA microplate reader (Thermo Fisher Scientific). The XOD activity was calculated as follows [19]:

$$\text{XOD activity (\%)} = \frac{X / X_C}{X_O / X_{CO}} \times 100, \quad (2)$$

where X is the absorbance of formazan in the *Ever-rose* extract, X_C is that of the *Ever-rose* extract, X_O is that of formazan in the control, and X_{CO} is that of the control.

2,2-diphenyl-1-picrylhydrazyl (DPPH) assay

The antioxidative potential of the *Ever-rose* extracts was evaluated using DPPH radical-scavenging capacity. A DPPH solution (0.1 mM) was prepared by dissolving DPPH in 80% ethanol. Subsequently, 20 µL of the sample solution was mixed with DPPH solution to achieve final concentrations of 50, 100, 500, and 1,000 ppm and then stirred vigorously. Next, the mixture was incubated in the dark for 30 min at room temperature. The absorbance of the reaction mixture was measured at 517 nm using an ELISA microplate reader (Thermo Fisher Science). The DPPH radical scavenging activity was determined as follows [20]:

$$\text{Inhibition ratio (\%)} = \frac{A_{CS} - A_S}{A_{CS}} \times 100, \quad (3)$$

where A_{CS} is the difference in absorbance between Blank_1 and Blank_2. Blank_1 contained no antioxidants,

whereas Blank_2 contained only the solvent used for the *Ever-rose* extract. A_S is the difference in absorbance between the *Ever-rose* extract and Blank_2.

Annexin V assay

The HDFs were maintained in DMEM supplemented with 10% FBS, 100 U/mL penicillin, and 100 µg/mL streptomycin at 37 °C under a humidified atmosphere of 5% CO_2. They were plated on 35 mm dishes at a density of 1.5×10^5 cells per dish. After 24 h of incubation, the cells with *Ever-rose* extracts (final concentration: 6.25 µg/mL, w/v) were exposed to infrared A (IRA) irradiation six times. The irradiation was performed on the transparent lids of the cell culture dishes using a customized solar IRA generator at an irradiance of 42 mW/cm^2 for 4 h/day, which is a protocol used in a previous study [21]. During the irradiation, the cell culture dishes were placed on a water-circulating plate equipped with a circulating water bath (LKlab Korea, Gyeonggi-do, Korea) at 34 °C. After the final irradiation, the cells were washed two times with PBS. Subsequently, they then stained with fluorescein isothiocyanate (FITC)-labeled annexin V in a binding buffer (10 mM HEPES [pH 7.4], 140 mM NaCl, and 2.5 mM $CaCl_2$) and incubated for 15 min at room temperature in the dark. FITC-labeled Annexin V Apoptosis Detection Kit I purchased from BD Biosciences (Franklin Lake, NJ, USA) was used. The non-irradiated cells at 37 °C and IRA-irradiated cells without rose extracts were similarly stained with FITC-labeled annexin V as the control. After washing with the binding buffer, the cells were washed with PBS containing 5% FBS. After the cells were fixed with formaldehyde (3.7%) in PBS solution for 10 min and coated with mounting solution, the fluorescence in the cells was visualized using an inverted fluorescence microscope (Olympus, Shinjuku, Tokyo, Japan). Additionally, the fluorescence intensity within the cells was quantified using the ImageJ software (National Institutes of Health, USA; http://rsb.info.nih.gov/ij/).

MitoSOX assay

The mitochondrial ROS was determined using a Mitosox™ Red mitochondrial superoxide indicator (Thermo Fisher Scientific) according to the manufacturer's protocol. Briefly, HDFs were plated on 35 mm dishes at 1.5×10^5 cells per dish. After 24 h, the cells within the *Ever-rose* extract solutions (final concentration: 6.25 µg/mL, w/v) were irradiated six times with IRA at 34 °C, as stated previously. After the final irradiation, the cells were washed with PBS solution and treated with MitoSOX (5 µM) solution for 10 min at 37 °C in a humidified atmosphere of 5% CO_2. After incubation, the cells were visualized using inverted fluorescence microscopy and the fluorescence intensity within the cells was quantified using ImageJ.

Atomic force microscopy (AFM)

The elastic properties of the HDFs were analyzed using (AFM, NANOStation II, Herzogenrath, Germany). HDFs images were acquired under liquid conditions (PBS solution) with a reflex-coated gold cantilever in contact mode (Budget Sensor, Bulgaria). The resolution and scan speed were 512×512 pixels and 0.2 lines/s, respectively. The Young's moduli of the HDFs were determined from the force–distance (FD) curves. The loading force and loading rate of the probe were set to < 10 nN and < 1 µm/s, respectively. The FD curve was analyzed using the Sneddon model [22]. The specifications of the cantilever used for the measurement were as follows: resonance frequency, 13 kHz (± 4 kHz); force constant, 0.2 N/m (± 0.14 N/m); length, 450 mm (± 10 mm); width, 38 mm (± 5 mm); and thickness, 2 mm (± 1 mm). The used tip featured a radius and height of 5 nm (± 1 nm) and 17 mm (± 2 mm), respectively.

Western blotting

After several washes with PBS, the HDFs were scraped into radioimmunoprecipitation assay buffer containing a protease inhibitor cocktail. The cells were centrifuged at 15,000 g for 5 min (4 °C) to separate F-actin and G-actin. For the Western-blot analysis, the G-actin and F-actin were loaded separately onto 12.5% polyacrylamide gels, and the resolved proteins were transferred onto nitrocellulose membranes. The membranes were blocked with 5% fat-free milk in PBS (pH 7.4) for 30 min at room temperature and incubated with anti-actin antibodies (Cytoskeleton Inc., Denver, CO, USA). The antibodies were mixed with Tris-buffered saline with Tween® 20 (TBS-T) at dilutions of 1/1,000 and 1/500. Finally, the membranes were incubated with an anti-actin primary antibody (1:500 dilution) at 4 °C for 16 h, washed four times with TBS-T, incubated for 1 h with a horseradish peroxidase-conjugated secondary antibody (Cell Signaling Technology), and washed five times with TBS-T. The target protein bands were visualized using an enhanced chemiluminescence kit (Thermo Fisher Scientific) and imaged using the Davinch-Chemi Chemiluminescence Imaging System (Davinch-K Co.). The protein levels were quantified using ImageJ.

Cellular senescence

The cellular senescence was analyzed using a beta-galactosidase (SA-β-gal) activity assay kit (Sigma, MO, USA). HDFs were seeded into culture dishes (diameter = 35 mm) at 4.5×10^5 cells/well. The cell culture medium was removed and the cells were washed with

1 mL of 1X PBS. Next, the HDFs were fixed with fixative solution III (0.5 mL) for 15 min at room temperature. The cells were washed two times with 1 mL of 1X PBS. Subsequently, the staining solution mix was added (staining solution I, staining supplement, and 20 mg/mL X-gal). The cells were incubated at 37 °C for 24 h and observed under a microscope for the development of blue color.

Statistical analysis

All the data were analyzed statistically and expressed as mean ± standard error of the mean. The analyses were performed using one-way ANOVA, and the statistical significance was set at $p < 0.05$. Note that $^{*}p \leq 0.05$, $^{**}p \leq 0.01$, $^{***}p \leq 0.001$, and $^{****}p \leq 0.0001$. The R program (version 4.0.0) was used for statistical analysis.

Results

Preparation and cytotoxicity of *Ever-rose* extracts

Four varieties of rose were developed and named *Ever-rose*. The four varieties were denoted as ER004, ER011, ER012, and ER015 (Fig. 1A). The petals and leaves of *Ever-rose* were dried separately. Their extracts were obtained using 30% ethanol under reduced pressure. The petal and leaf extracts of ER004 were named ER004(P) and ER004(L), respectively, and those of the other rose species were named similarly. The dried extracts were dissolved in three solvents (DMSO, MeOH, and distilled water (DW)) at an extract concentration of 5 mg/mL (w/v) (Fig. 1B). As shown in Fig. 1B, the extract solution in DW did not precipitate in the samples, whereas aggregation was observed in the samples dissolved in MeOH. Therefore, the extracts were dissolved in DW and DMSO for the subsequent assays.

To evaluate the cytotoxic effects of the extracts on the HDFs, we measured the cell viability by increasing the extract concentration to 500 ppm. Different types of petals were observed, which showed different cytotoxicity levels (Fig. 1C). For the cells treated with ER004(P), the viability decreased gradually as the extract concentration increased, whereas treated with ER011(P) exhibited a decrease in viability of less than 18% up to a concentration of 100 ppm. However, at higher concentrations (> 200 ppm), the viability decreased by 43% compared with the control. The viability of HDFs treated with ER012(P) and ER015(P) did not vary significantly up to 300 ppm and decreased marginally above 400 ppm. No difference in cellular cytotoxicity was indicated among the leaf types (Fig. 1D). Regardless of the leaf type, the

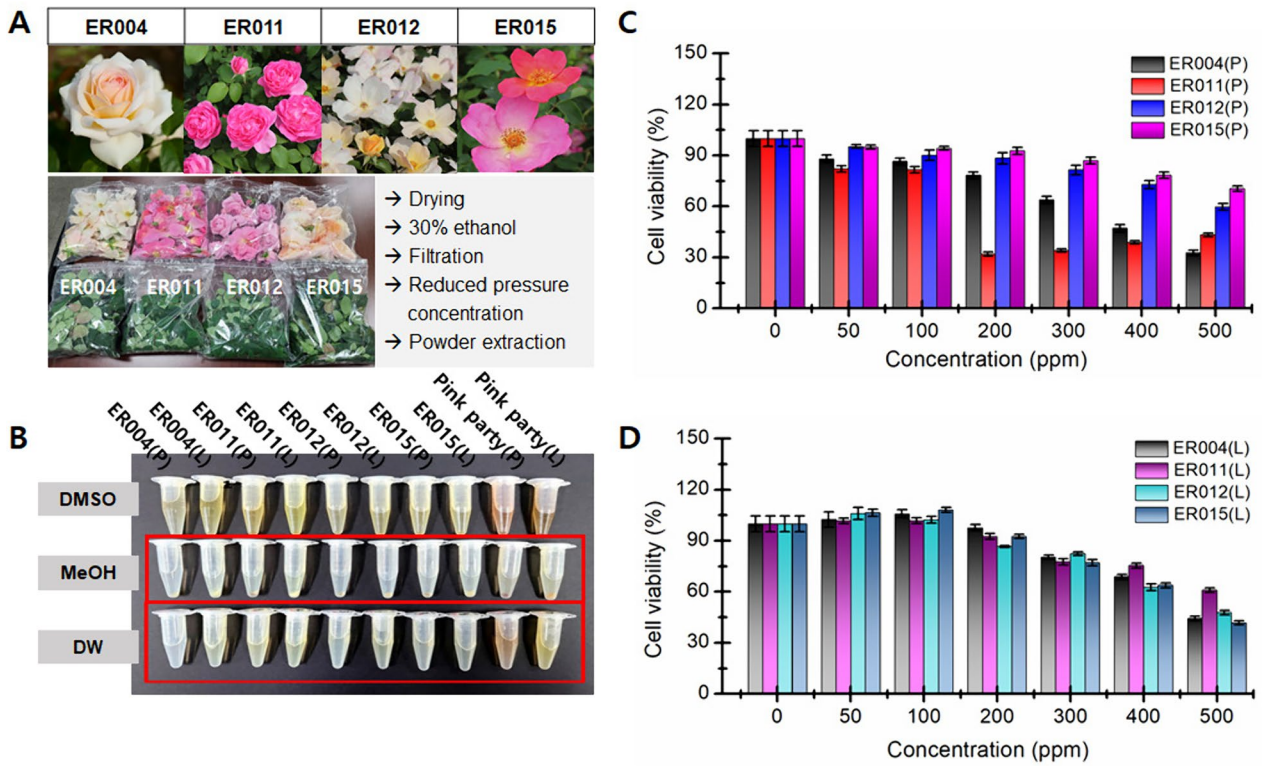

Fig. 1 **A** Four *Ever-rose* varieties, denoted as ER004, ER011, ER012, and ER015, were developed. Petal and leaf extracts of *Ever-rose* were obtained separately using 30% ethanol under reduced pressure. **B** Extracts were dissolved in DMSO, MeOH, and distilled water (DW). **C** Cytotoxic effect of extracts was evaluated by increasing extract concentration up to 500 ppm. **D** Cytotoxic effect of *Ever-rose* leaf extract was evaluated separately

viability of the treated HDFs varied marginally up to 100 ppm and then decreased gradually at concentrations above 200 ppm.

Chemical analysis of *Ever-rose* extracts

The petal extracts were chemically analyzed using UHPLC-triple TOF–MS/MS. The total positive ion chromatograms of ER004(P), ER011(P), ER012(P), and ER015(P) are shown in Fig. 2A–D, respectively. All the extracts showed similar responses in both the positive and negative ion modes and exhibited similar chromatograms (Fig. S1). Based on the mass, retention times (RTs), and MS/MS spectra, we putatively identified 29 compounds [23, 24], including chlorogenic acid, cyanidin, and kaempferol (Table S1).

The contents of the chemical compounds varied across the rose varieties (Fig. 2E–H). Kaempferol (3,4′,5,7-tetrahydroxyflavone) is a natural flavanol observed in various plants. Several kaempferols and their derivatives including kaempferol 3-(6"-acetylglucoside), kaempferol 3-glucuronide, and kaempferol-3-O-rutinoside were identified. These components were present at relatively low levels ($< 10 \times 10^5$) in ER004(P), ER011(P), ER012(P), and ER015(P). Kaempferol-3-O-rutinoside (RT = 7.52) was abundant in ER004(P), whereas kaempferol diglucoside (RT = 6.25) and kaempferol rhamnoside (RT = 9.34) were abundant in ER011(P) (Fig. 2E, F). Quercetin is a widely distributed flavanol in plants. It was present at relatively low levels in ER004(P), ER011(P), and ER012(P). However, quercetin 7-O-glucoside (RT = 6.86) was found to be abundant in ER015(P) (Fig. 2H). Cyanidins are a natural organic compound with potent antioxidant activity. It was present at similar levels in all four petal extracts. However, cyanidin 3-glucoside (RT = 7.86) was particularly abundant in ER004(P) and ER012(P) (Fig. 2E, G).

Antioxidant effects of *Ever-rose* extracts

Free radicals are the major cause of skin aging [25]. The antioxidant effect of the rose extract on free radical scavenging was analyzed by measuring the SOD activity, XOD activity, DPPH inhibition.

SOD removes excess ROS from the body by catalyzing an unbalanced reaction that converts superoxide ions into oxygen and hydrogen peroxide [26]. Increased SOD activity prevents or reduces wrinkles by scavenging free radicals [26]. Therefore, substances with SOD activity are suitable as antihypertensive drugs or cosmetic additives for preventing skin aging [27]. Figure 3A shows the SOD activity of the petal extract and control sample. In the control group, green tea indicated more significant SOD activity than Pink party and retinol acid at both 100 and 500 ppm. Similarly, the SOD activity for green tea was higher than that in the *Ever-rose* extract. Note that retinol was treated with 50 and 100 ppm concentrations. At a concentration of 100 ppm, the ER011(P) extract showed the highest SOD activity (18.1%), whereas the other groups showed similar levels of activity (10.2–12.7%). In

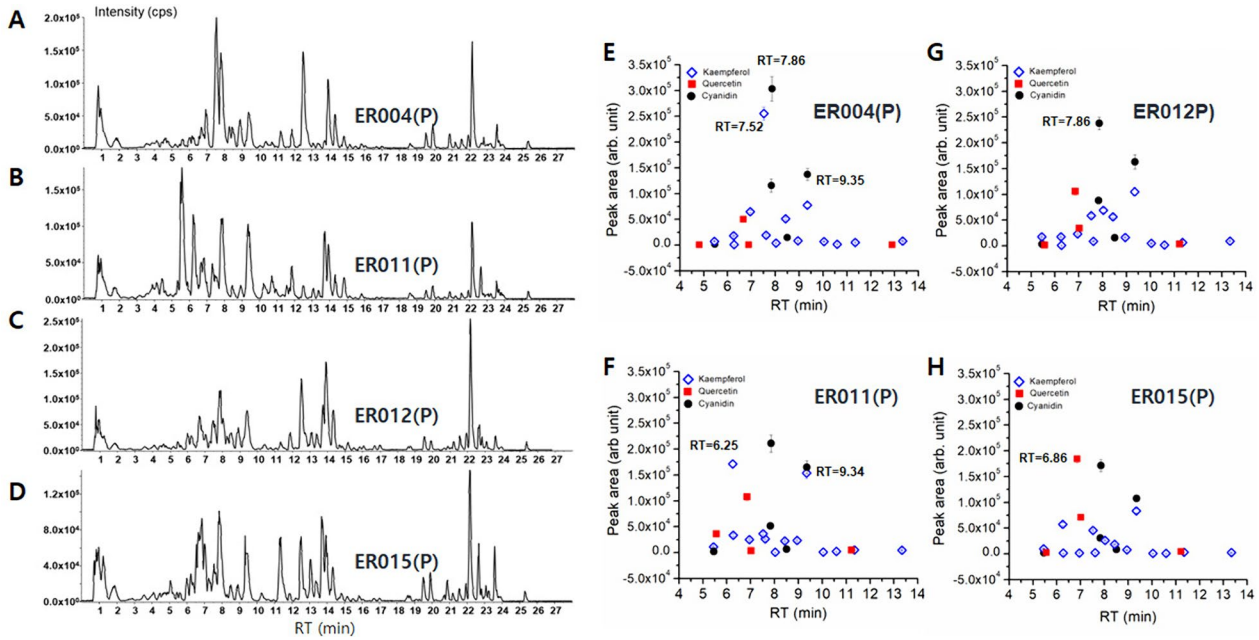

Fig. 2 LC–MS/MS chromatograms of *Ever-rose*. Representative base peak chromatograms of **A** ER004, **B** ER011, **C** ER012, and **D** ER015 obtained in positive ion mode. **E**–**H** Type and amount of antioxidants identified in ER004(P)–ER015(P), respectively

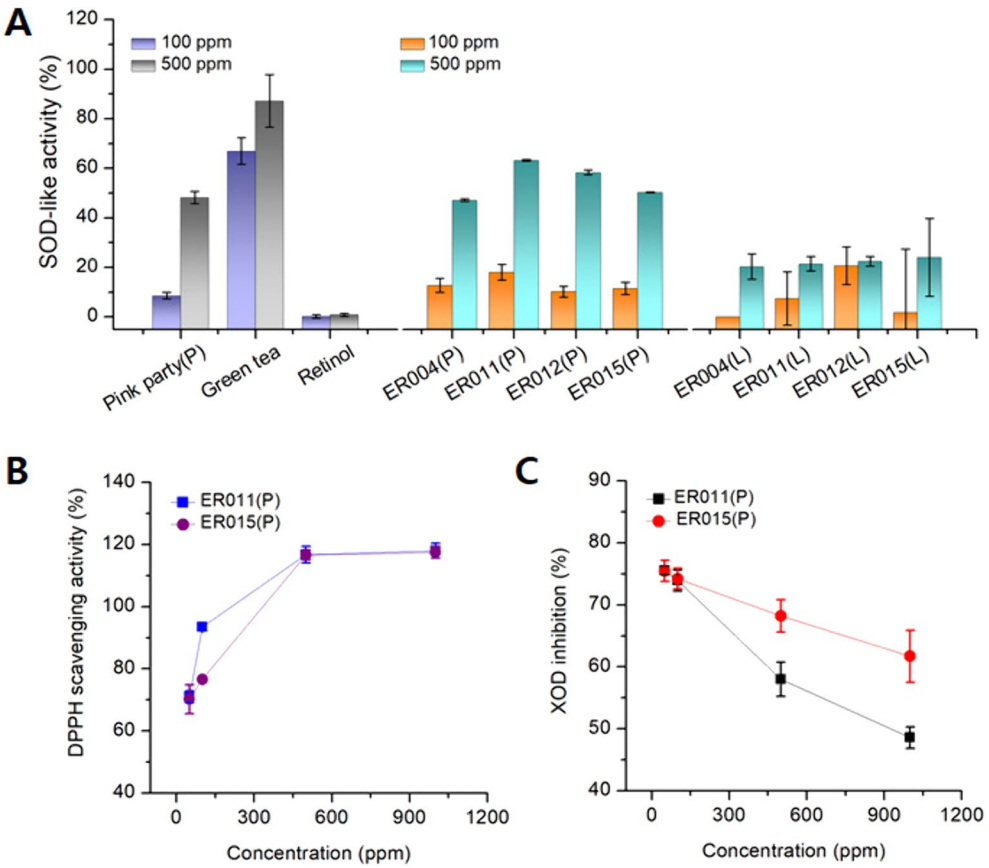

Fig. 3 **A** SOD-like activity of petal and leaf extracts of *Ever-rose* at concentrations of 100 and 500 ppm. SOD-like activity of Pink party roses, green tea, and retinol were evaluated as controls. **B** DPPH free-radical scavenging activity of petal extracts of ER011 and ER015 at concentrations of 50, 100, 500, and 1000 ppm. **C** Xanthine oxidase (XOD) activity inhibition of petal extracts of ER011 and ER015 at concentrations of 50, 100, 500, and 1,000 ppm

all the groups treated with the petal extract at a concentration of 500 ppm, the SOD activity increased to 3.5–5.7 times that of the case at a concentration of 100 ppm. Among the leaf extracts, the ER012(L) and ER015(L) extracts exhibited the highest (20.7% at 100 ppm) and lowest (1.9%) activity, respectively. At 500 ppm, the SOD activity was similar for all the samples (20–24%).

The most common action mechanism of antioxidants is their reaction with free radicals. Free radical-scavenging activity is a measure of the antioxidant effect or the suppression of aging in the human body by the donation of electrons to active radicals [28]. DPPH free-radical scavenging assay is widely used to monitor the antioxidant activity of plant extracts [29, 30]. Petal extracts ER011(P) and ER015(P) showed increased scavenging activity against DPPH free radicals in a dose-dependent manner (Fig. 3B), whereas their scavenging activities did not differ significantly. XOD contributes significantly to the cellular oxidative status, aldehyde detoxification, oxidative damage during ischemia–reperfusion, and neutrophil mediation by generating ROS [31]. As shown in Fig. 3C, ER011(P) and ER015(P) inhibited the XOD activity in a dose-dependent manner. Notably, ER011(P) showed a more prominent level of inhibitory activity than ER015(P).

Effects on MMP-1 expression and collagen production

Irradiating HDFs with UVB light causes intracellular DNA damage and photoaging, which consequently inhibits cell growth and increases MMP expression [32, 33]. MMP-1 is a proteolytic enzyme that can degrade native fibrillar collagen, particularly type-I and -III fibrillar collagen, in the human skin [34, 35]. These fragments subsequently undergo unfolding and degradation promoted by MMP-2, MMP-9, and MMP-3 [36]. Therefore, MMPs contribute significantly to wrinkle development [37]. When the HDFs were irradiated with UVB (Cont_2), the MMP-1 expression increased by almost twice compared with that in the HDFs that were not irradiated with UVB (Cont_1) (Fig. 4A). In the positive control group treated

with Pink party (P) and green tea, the MMP-1 expression was suppressed compared with that in Cont_2 at both 10 and 50 ppm, notwithstanding the UVB treatment. However, retinol was ineffective in inhibiting the MMP-1 expression. When the UVB-irradiated HDFs were treated with the petal extract, their MMP-1 expression was suppressed significantly in all the cases. The cells treated with 10 ppm ER004(P) and ER015(P) showed MMP-1 expression levels similar to those for Cont_1 cells. The MMP-1 expression levels in the cells treated with ER011(P) and ER012(P) at 10 ppm were 20–30% lower than those for Cont_1. At a high concentration of 50 ppm, the MMP-1 expression in the petal extract-treated HDFs reduced by 10%–37% compared with that of Cont_1. Additionally, the leaf extracts inhibited MMP-1 expression induced by UVB irradiation. However, the effect was modest compared with that of the petal extracts.

Procollagen type I is an extremely important indicator of skin aging and is caused by the accumulation of damaged collagen [38]. The *Ever-rose* petal extracts promoted collagen production in the HDFs (Fig. 4B). Compared with the control group, ER011(P) treatment increased collagen synthesis by 97% at a low concentration of 10 ppm and by 67% at a high concentration of 50 ppm. In the HDFs treated with the other petal extracts (ER004(P), ER012(P), and ER05(P)), the collagen synthesis was lower than that in the cells treated with ER004(P). However, it was 22%–56% higher than that in the control group. Similarly, the leaf extracts stimulated collagen synthesis. The stimulatory effects of the different leaf types were similar to those of the petal extracts. The positive controls were less effective than *Ever-rose* in synthesizing collagen type I.

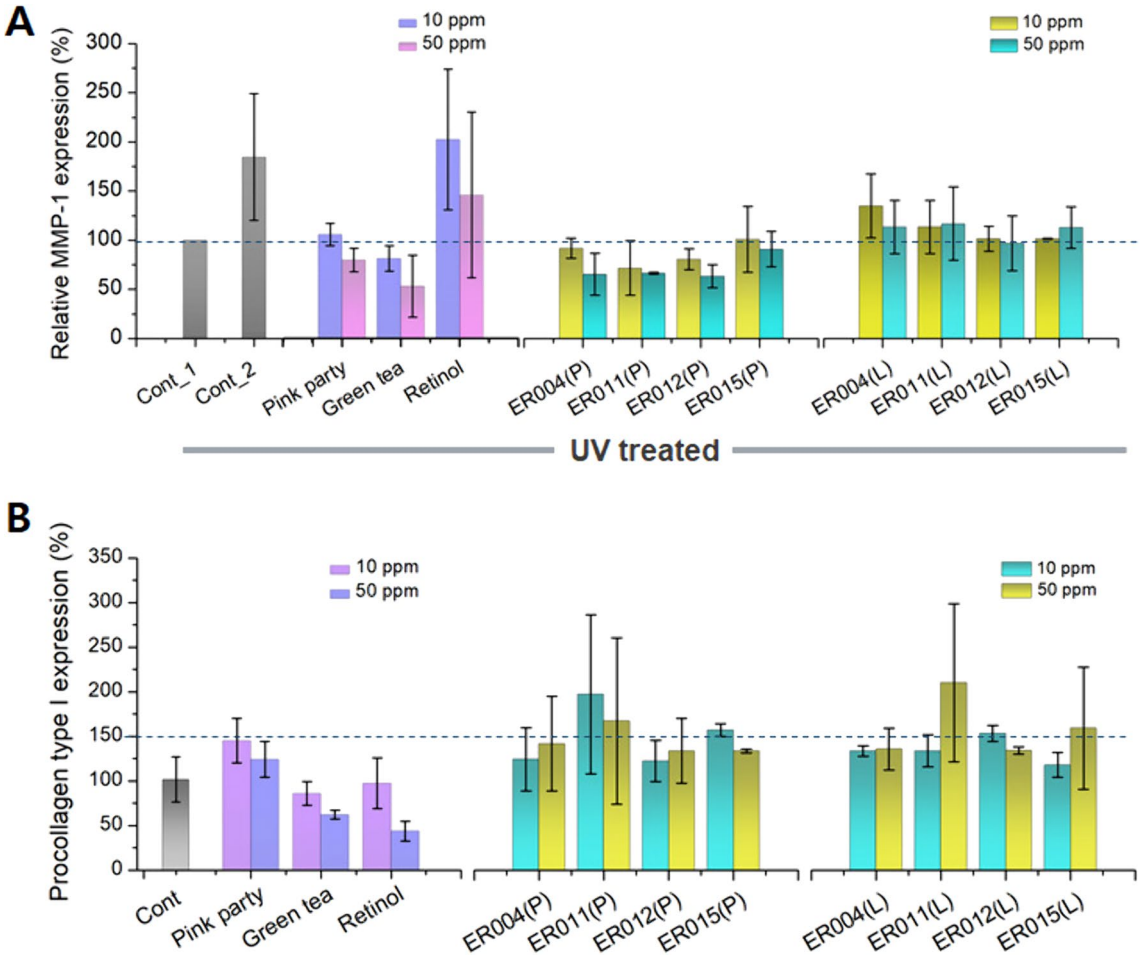

Fig. 4 **A** Inhibition of UVB-induced MMP-1 production by *Ever-rose* in human dermal fibroblasts. Fibroblasts not irradiated with UVB and irradiated cells are denoted as control_1 (Cont_1) and control_2 (Cont_2), respectively. Effects of Pink party rose, green tea, and retinol on UVB-induced MMP-1 production were compared. **B** Effects of *Ever-rose* on procollagen type I expression. HDFs treated with Pink party rose, green tea, and retinol were considered positive controls. HDFs were treated with *Ever-rose* petal and leaf extracts at 10 and 50 ppm, respectively

Protective activity by rose extracts against IRA

Based on our previous study, chronic IRA exposure can induce severe cellular damage (including apoptosis) and increased mitochondrial ROS levels in HDFs [39]. To investigate the protective activity of *Ever-rose* extracts against chronic IRA exposure, the extent of apoptotic signals and mitochondrial ROS levels after IRA irradiation was examined in HDFs. To visualize apoptotic cells, annexin V with a green fluorescent dye was used as an apoptosis marker because of its specific attachment to phosphatidylserine [40]. Figure 5A shows the fluorescence images of HDFs treated with petal extracts after IRA irradiation. During IRA irradiation, the HDFs were incubated with rose extract at 6.25 ppm in 10% FBS-containing medium. After this irradiation (Cont_2), the cellular green fluorescence intensity increased significantly compared with the case of Cont_1. However, the cells treated with *Ever-rose* petal extracts and Pink party (P) showed attenuated fluorescence signals. The levels of fluorescence intensity with annexin V were analyzed quantitatively. As shown in Fig. 5B, the relative intensity of annexin V increased 3.1-fold by IRA irradiation compared with that for Cont_1. However, the enhanced apoptotic signals induced by IRA irradiation were downregulated significantly by the treatment with the rose extracts. In particular, the fluorescence intensities of ER012(P)-, ER015(P)-, ER015(L)-, and Pink party(P)-treated cells were 91.3 ± 35.3, 104.9 ± 51.1, 136.4 ± 89.2, and 107.1 ± 33.9, respectively. These values are comparable to that of the IRA-untreated cells.

After photo-irradiation, the mitochondrial ROS levels increase significantly, which causes inflammation, mitochondrial dysfunction, cellular damage, and eventually apoptosis [41, 42]. To assess the cellular damage by IRA irradiation, the mitochondrial ROS levels were measured using the MitoSOX assay. As shown in Fig. 5C, the IRA irradiation significantly increased the levels of red fluorescence signals induced by mitochondrial ROS. However, the treatment with rose extract decreased the mitochondrial ROS levels compared with those in the IRA cells. Subsequently, the relative red fluorescence intensity was analyzed quantitatively (Fig. 5D). Most of the cells treated with the rose extract exhibited reduced mitochondrial ROS levels. The red fluorescence intensities of the cells treated with rose extracts ER012(P), ER012(L), ER015(P), ER015(L), Pink party(P), and Pink party(L) were 105.2 ± 32.3, 151.2 ± 30.4, 126.6 ± 42.2, 80.9 ± 23.5, 109.5 ± 36.8, and 174.7 ± 42.8, respectively, with the fluorescent level of cell being 100. ER012(L), ER015(P), and Pink party(L) showed a milder reduction in mitochondrial ROS than the other rose extracts. In particular, rose extracts ER012(P), ER015(L), and Pink party(P) alleviated IRA-induced photodamage in skin cells by suppressing apoptotic signaling and decreasing the mitochondrial ROS levels.

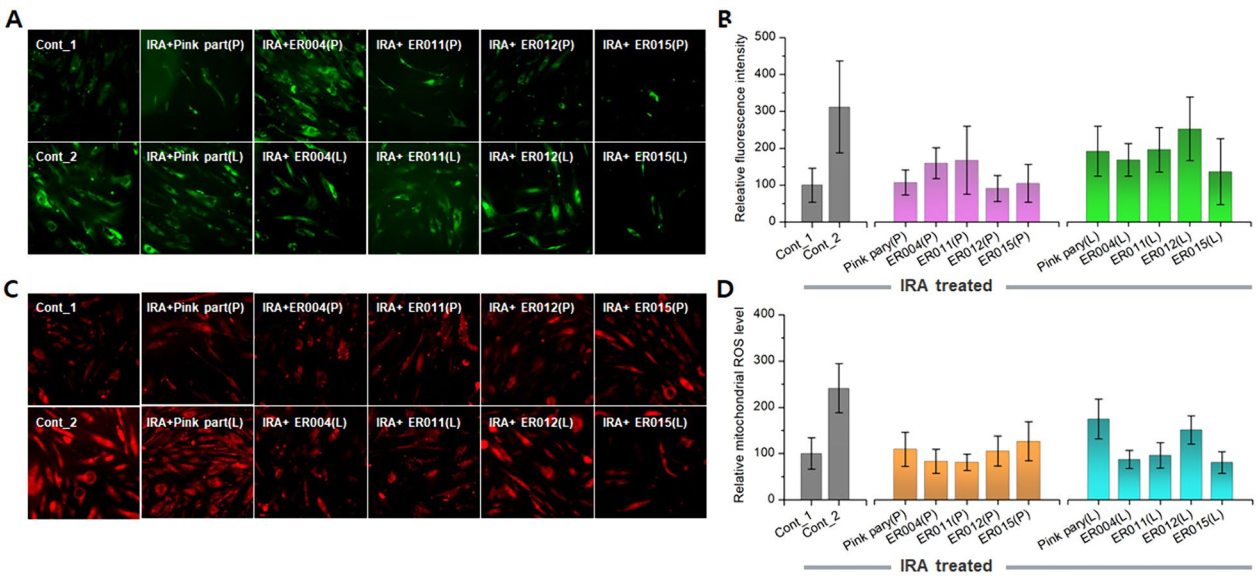

Fig. 5 **A** Annexin V-FITC fluorescence of fibroblasts treated with Pink party and *Ever-rose* extracts (6.25 ppm) after IRA irradiation was imaged. Fibroblasts not irradiated with IRA and irradiated cells are denoted as control_1 (Cont_1) and control_2 (Cont_2), respectively. **B** Quantitative analysis of annexin V-FITC fluorescence intensity after IRA irradiation. **C** Mitochondrial superoxide production detected using MitoSOX via confocal microscopy. Representative image of MitoSOX red staining of superoxide radicals in fibroblasts. **D** Effects of *Ever-rose* on mitochondrial ROS accumulation induced by IRA irradiation

Variations in cellular elasticity induced by *Ever-rose* extracts

The cellular elasticity was investigated using AFM. We first obtained a high-resolution AFM image of the HDFs (Fig. 6A, B), followed by the FD curves from the body region. The FD curves were measured at approximately 10 locations in each cell and approximately 20 or more cells in each group. Figure 6C shows the FD curve measured for the control cells. The gray circles and rectangles represent the approach and retraction processes, respectively. The Young's modulus of each cell was calculated from the approach curve using the Sneddon model, as shown by the dotted red line [43]. Figure 6D shows the distribution of the Young's modulus measured in the control cell group. Even within a group, the Young's modulus showed a wide distribution, thus indicating the inhomogeneous elastic characteristic of the cells. The Young's modulus is the ratio of stress (force applied per unit area) to strain (deformation by stress). Therefore, a high Young's modulus indicates that a large stress is required for cell deformation to occur [44]. In other words, the cells with a high Young's modulus are rigid and do not deform well. However, a low Young's modulus indicates that the cells can be deformed even under small stresses. Therefore, the cells with low Young's moduli are soft.

The petal extracts altered the cellular elasticity. Compared with the control, the Young's modulus of the cells treated with the petal extract decreased by 40–54% (Fig. 6E). The reduction in the HDFs treated with ER011(P) was particularly evident. By contrast, the cells treated with the leaf extract did not show a significant variation in the Young's modulus, except for those treated with ER004(L) (Fig. 6F). Because the cellular elasticity is primarily determined by the F-actin content, the F-actin content was analyzed in both the cells treated with petal and leaf extracts (Fig. 6G). The HDFs treated with the petal extract showed a decrease in F-actin content compared with the control cells (Fig. 6H). The cells treated with ER015(P) showed the highest reduction (40%), whereas those treated with ER004(P) showed the lowest reduction (16%). The F-actin content of the cells treated with the leaf extract was higher than that of the control, which is inconsistent with the elasticity results (Fig. 6I). However, the actin content between leaf types remained the same.

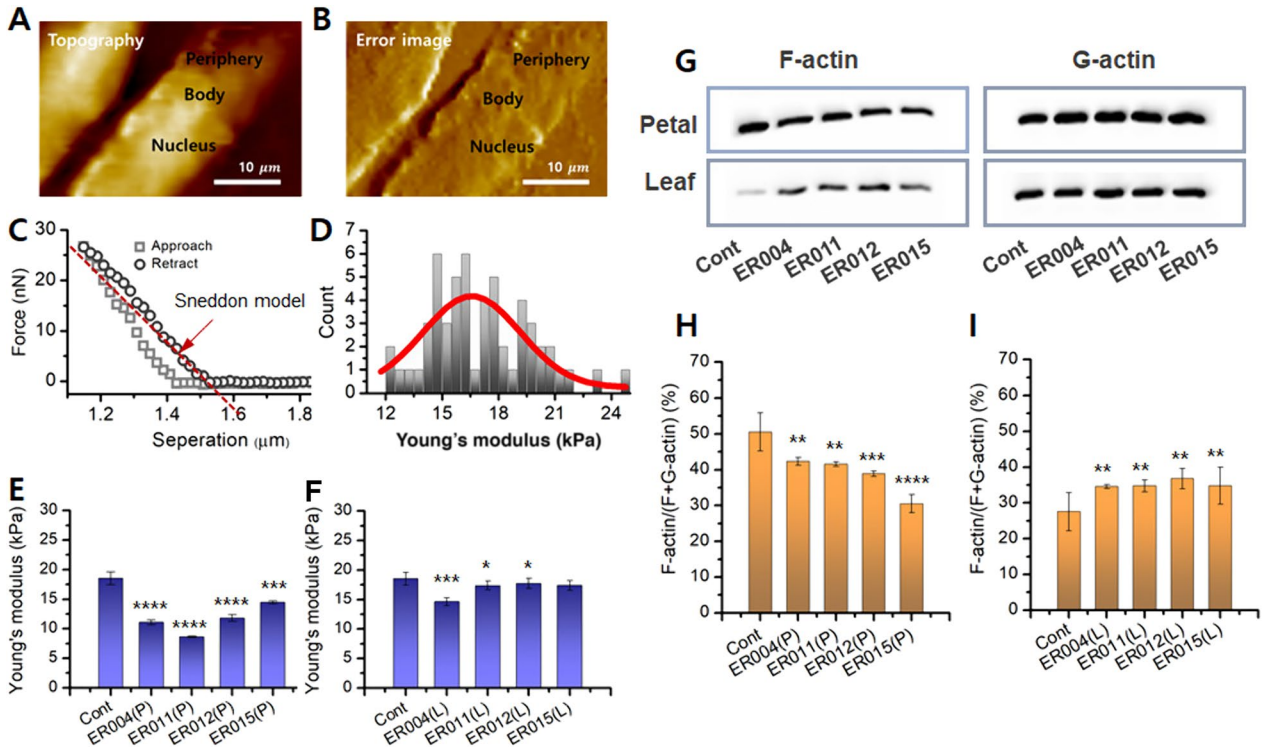

Fig. 6 Representative AFM images of fibroblasts: **A** Topography and **B** error image. **C** FD-curve measured on control cell. **D** Distribution of Young's modulus measured in control cell. Young's modulus of cells treated with *Ever-rose* **E** petal and **F** leaf extracts (100 ppm). **G** F-actin content in fibroblast treated with *Ever-rose* petal and leaf extracts (100 ppm). Quantitative analysis of F-actin content in fibroblast treated with *Ever-rose* **H** petal and **I** leaf extracts. Pink party rose and DMSO were regarded as positive and negative controls, respectively. Error bars indicate mean ± SD (*$p \le 0.05$, **$p \le 0.01$, ***$p \le 0.001$, and ****$p \le 0.0001$)

Effect of *Ever-rose* extracts on cell-shape variations caused by aging

The elasticity of a single cell varies with age. In general, younger cells have lower Young's moduli and deform more straightforwardly. However, older cells have higher Young's moduli and are more rigid. To examine the effect of *Ever-rose* on the variations in cellular elasticity with age, the cells were aged from passage 4 to passage 16 (p4 to p16). Based on the results of previous experiments, we selected two petal extracts, ER011(P) and ER015(P), as they induced the largest and smallest variations in cell elasticity, respectively.

First, we analyzed the SA-β-gal activity to determine whether an increase in the number of cell passages induces senescence. SA-β-gal is a hydrolase enzyme originating from β-gal in lysosomes that catalyzes the hydrolysis of β-gal into monosaccharides [44]. The optimal pH for activating β-gal is 4.5. However, in senescent cells, it is activated at pH 6.0 owing to increased lysosomes [45, 46]. The SA-β-gal activity was investigated in five cell groups: control cells (Cont; untreated) and retinol-, DMSO-, ER011(P)-, and ER015(P)-treated HDFs (Fig. 7A). Because the petal samples were extracted with DMSO, cells treated with 20% DMSO were investigated as negative control (Ncont), whereas the HDFs treated with retinol (20 μM) were regarded as positive control (Pcont). Retinol, which is derived from vitamin A, is an effective anti-aging and skin-regenerative ingredient [47]. It increases skin-cell turnover and stimulates collagen production to maintain the elasticity and firmness of skin. SA-β-gal positive cells were observed frequently at p12 in four groups (Cont and Retinol-, DMSO-, and ER02(P)-treated HDFs). Positive cell staining was infrequent in the early passages of p4 and p8 cells (Fig. S2). At the subsequent passages of p12 and p16, all the groups showed similar levels of SA-β-gal positive cell staining (Fig. 7A).

Additionally, aging induces variations in cell size and morphology. Cells enlarge in vitro and in vivo when entraining senescence aging [48]. Aged cells can be two to three times as large as young cells. In all the groups, we examined the variations in the cell size and height in response to increased passages. The size of the HDFs was measured using an optical microscope, and their height was determined from AFM images (Fig. 7B, C). The cell height was defined as the difference between the matrix and nucleus in the z-axis direction (Fig. 7D).

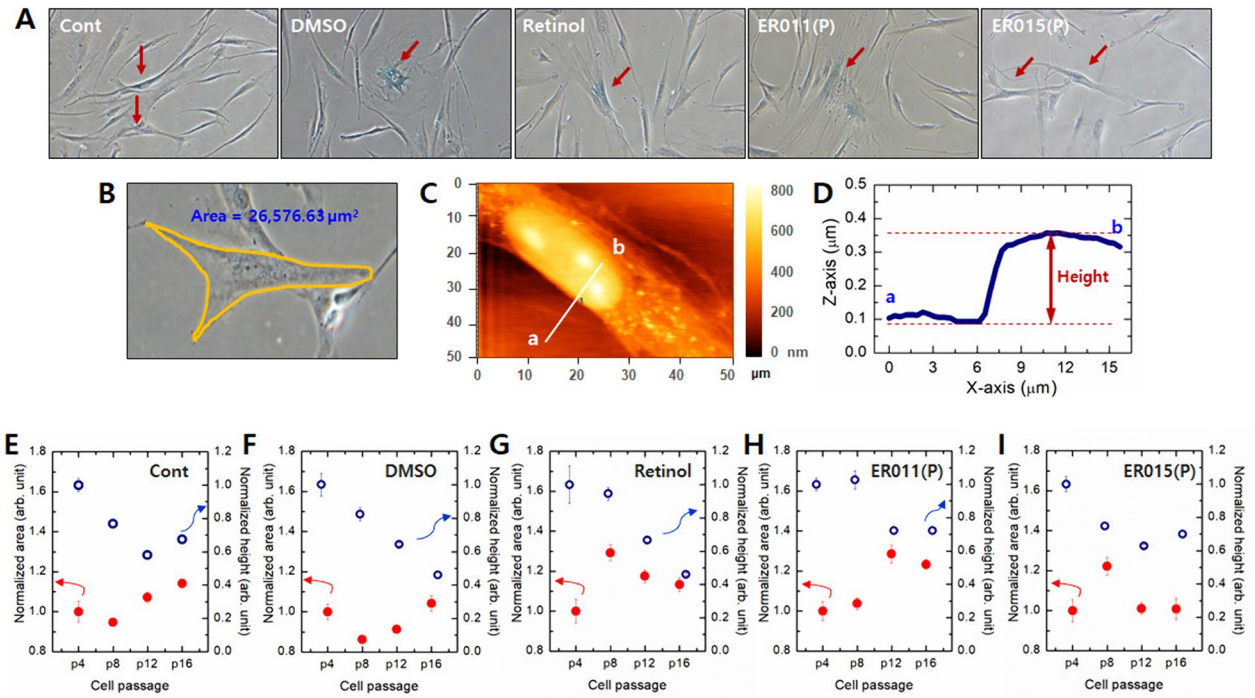

Fig. 7 **A** SA-β-gal activity in untreated fibroblasts (Cont) and fibroblasts treated with retinol, DMSO, ER011(P), and ER015(P), respectively. Concentrations of retinol, ER011(P), and ER015(P) were 20 μM, 100, and 100 ppm, respectively. **B** Morphological variations in cell size with aging measured using light microscopy and ImageJ program. **C** Cell height was defined as the difference between the matrix and the nucleus in the z direction along line a-b in the AFM images. **D** The cell height can be determined from the profile of lines a-b. Variations in cellsize and height in **E** Cont, **F** DMSO, **G** retinol, **H** ER011**P**, and **I** ER015(P) groups

In all the groups, the cell size and height varied over time. However, the extent of variation varied between groups. In the Cont and DMSO-treated groups, the cell size at p8 decreased compared with that at p4. Subsequently, it increased with the number of passages (Fig. 7E, F and S3). In the Pcont group, the cell size increased at p8 compared with that at p4. However, it decreased as the number of passages increased further (Fig. 7G). The ER011(P) and ER015(P) groups treated with the petal extract showed a marginal increase in cell size at p8 compared with that at p4. However, this increase was not sustained when the number of passages increased (Fig. 7H, I). The variations in the cell size appeared to be inhibited by retinol and rose-extract treatments under a high number of passages. Although the total cell volume did not remain constant, the height generally decreased as the cell size increased. Thus, the variation in the cell height with the number of passages was opposite to that in the cell size in most of the groups (Cont, DMSO, ER02(P), and ER04(P)). In the retinol-treated group, although the cell size decreased under a high number of passages, the height decreased as age increased. These results indicate that the *Ever-rose* extract is effective in inhibiting age-related variations in cell morphology.

Efficiency of *Ever-rose* in restoring elasticity of aged cells

We measured the Young's modulus under various passages of the HDFs. As mentioned above, the HDFs became rigid as the number of passages increased (Fig. 8A). Furthermore, the Young's modulus was altered by external factors such as DMSO, retinol, and *Ever-rose* extracts. For a comparative analysis of the efficacy of the *Ever-rose* petal extracts based on the number of cell passages, we normalized the Young's modulus of each group (ER011(P), ER015(P), DMSO, and Retinol) to that of the control. Figure 8B shows the normalized Young's modulus as a function of the cell passage. In the ER011(P)-treated cells, the Young's moduli of the p4 and p16 cells were higher than those of the control, whereas those of the p8 and p12 cells were lower than those of the control. The Young's modulus of the ER015(P)-treated cells varied similarly to that of the ER02(P)-treated cells, whereas that of the DMSO-treated group varied similarly to that of the cells treated with petal extracts. However, the variation degrees were different. Therefore, the variation in

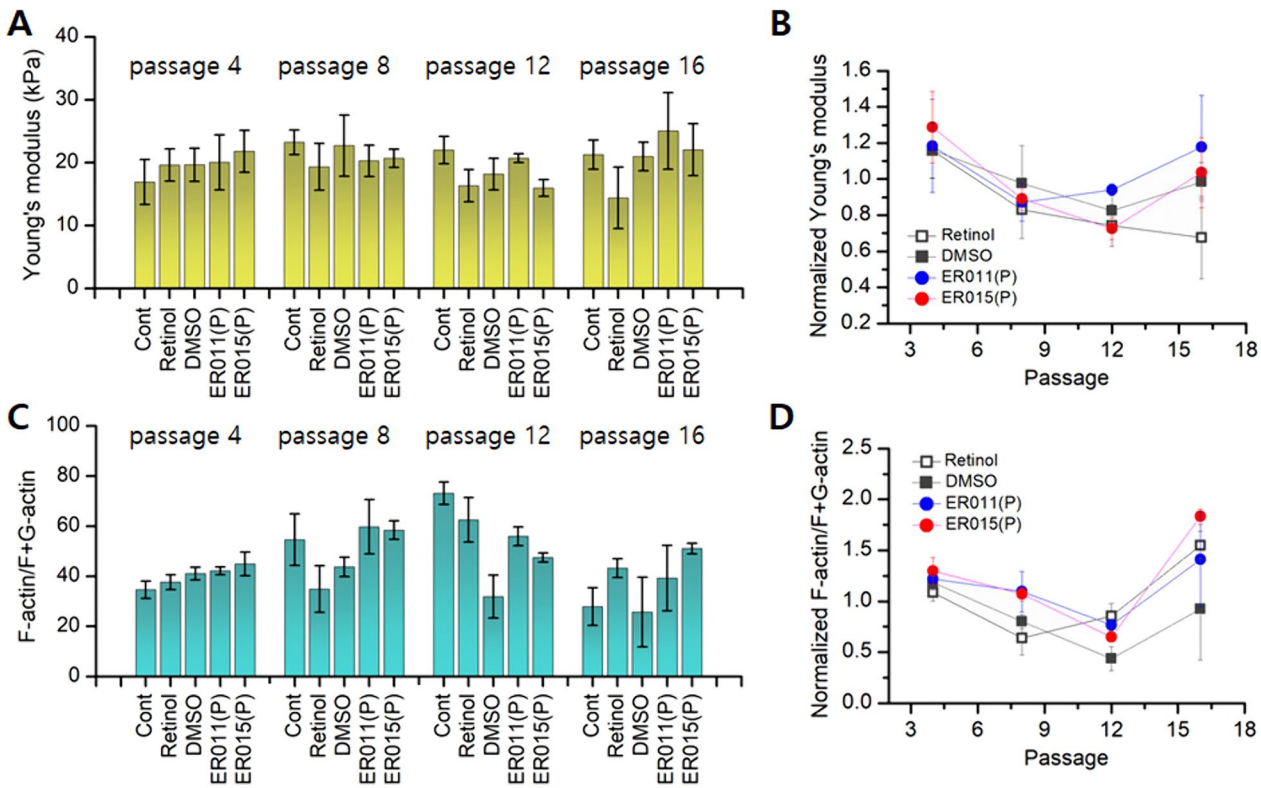

Fig. 8 **A** Variations in Young's modulus with aging in **E** Cont, **F** DMSO, **G** retinol, **H** ER011(P), and **I** ER015(P) groups. **B** Age-dependent variation in Young's modulus normalized to control. **C** Variations in F-actin with aging in **E** Cont, **F** DMSO, **G** retinol, **H** ER011(P), and **I** ER015(P) groups. **D** Age-dependent variation in F-actin normalized to control

the Young's modulus with the number of passages is attributable to the effect of the *Ever-rose* petal extract. In all the groups, the F-actin content varied with the number of cell passages, whereas the age-related variations in F-actin were generally similar to those in the Young's modulus (Fig. 8C). In the control group, the F-actin content increased until p12 and then decreased at p16. Compared with the control group, the F-actin content in the DMSO-, ER011(P)-, and ER015(P)-treated groups decreased until p12 and then increased at p16 (Fig. 8D). In the retinol-treated group, the normalized F-actin levels decreased until p8 and then increased beginning from p12 (Fig. 8D). The arrangement or distribution of F-actin after cell passaging or treatment did not vary significantly (Fig. S4). Based on the results above, we hypothesize that cell elasticity is specifically regulated by *Ever-rose* at a specific age. *Ever-rose* appeared to be unsuitable for regulating the elasticity of excessively young or excessively old cells. However, applying *Ever-rose* to middle-aged cells appeared to effectively restore elasticity.

Discussion

The skin is the largest organ in the body. It is subjected to aging mechanisms under the influence of both intrinsic (chronological aging, genetics, etc.) and extrinsic factors (e.g., environmental) [11, 12]. Natural products contain significant amounts of biologically active substances and have few side effects on the human body. Therefore, they are being continuously researched and developed as raw materials for anti-aging products.

ROS such as superoxide anions and hydrogen peroxide are generated during normal cellular processes or can be generated excessively in response to environmental stress. Although ROS are not strong oxidants, they can be converted to more unsafe oxidants through hazardous reactions in tissues [49]. The oxidative stress initiated by ROS can contribute to skin aging by activating enzymes such as hyaluronidase, collagenase, and elastase. This deteriorates specific molecules contributing to skin moisture or mechanical properties [50]. Therefore, their antioxidant properties have been prioritized in the development of anti-aging products.

Roses are well-known natural antioxidants with abundant bioactive substances such as polyphenols and phenolic compounds. They have been used in cosmetics and medicine since times immemorial. The newly developed *Ever-rose* demonstrates remarkable antioxidant properties. The petal extracts of the *Ever-rose* variants showed SOD activity superior to that of retinol and comparable to that of Pink party. Their DPPH free-radical scavenging activity is dose dependent and occurs at higher rates compared with those of other antioxidants such as ascorbic acid [51]. The *Ever-rose* petal extract effectively inhibited the MMP-1 expression induced by UVB. This resulted in the higher expression of collagen type I as compared with the control group. After IRA irradiation, the mitochondrial ROS levels did not increase and apoptotic signaling was inhibited in the cells treated with the *Ever-rose* extract. Morphological and mechanical variations in the HDFs caused by aging were inhibited or reversed by the *Ever-rose* extract. The Young's modulus of the HDFs treated with the petal extract was lower than that of the control cells. This indicates that the cells were softened by *Ever-rose*. Furthermore, the *Ever-rose*-treated cells differed from the control cells in terms of the variations in the area and height as the number of passages increased.

The anti-aging and antioxidant advantages of *Ever-rose* were the most evident in the flowers and less significant in the leaves. Moreover, ER011(P) showed the best characteristics. In all the antioxidant-activity assessments, ER011(P) surpassed ER005(P), ER012(P), and ER015(P) by 22–38%. The cell elasticity was approximately twice higher than that of the control. To examine the superior properties of ER011(P), we analyzed its chemical composition using UPLC-Triple TOF–MS/MS.

Among the identified compounds listed in Table S1, ER011(P) contained 4 cyanidin, 14 kaempferol, and 3 quercetin compounds. Cyanidins belong to the anthocyanin group and possess antioxidant and radical-scavenging properties [52]. Kaempferol and quercetin are natural flavanols present in various plants with remarkable anti-inflammatory and antioxidant properties [53, 54]. Compared with ER015(P), which showed relatively low anti-aging and antioxidant activities, ER011(P) indicated more antioxidants (Fig. 9A). In ER015(P), only a few components, including kaempferol 3-glucuronide, were abundant. A comparison of the compound content ratios of the variants revealed that ER011(P) had a relatively high antioxidant content. In ER011(P), the content of 15, 11, and 16 compounds was found to be higher compared to ER004(P), ER012(P), and ER015(P), respectively (Fig. 9B). In ER004(P), ER012(P), and ER015(P), the contents of 10 compounds were lower than those in ER011(P) (Fig. 9B). Although this cannot be verified because many compounds have not been identified, relatively high amounts of anthocyanins and phenolic compounds may be responsible for the remarkable antioxidant and anti-aging properties of ER011(P).

Conclusions

In this study, we developed four new rose varieties (named *Ever-rose*) and evaluated their antioxidant and anti-aging activities. The petal extracts of *Ever-rose* showed favorable antioxidant activities in various assays, including SOD activity, DPPH free-radical

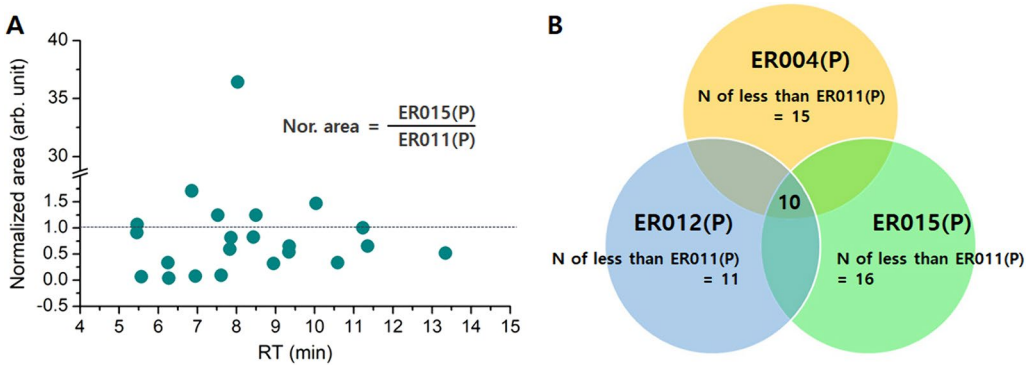

Fig. 9 Among the identified compounds, ER02(P) contains 4 cyanidin, 14 kaempferol, and 3 quercetin compounds. **A** Quantitative comparison of identified antioxidants in ER011(P) and ER015(P). **B** Number of antioxidants in ER004(P), ER012(P), and ER015(P), which is lower than that in ER02(P)

scavenging activity, and XOD inhibition. The MMP-1 expression after UVB irradiation and the mitochondrial ROS levels after IRA irradiation were inhibited effectively by the *Ever-rose* petal extracts. Treatment with *Ever-rose* petal extracts increased the elasticity of fibroblasts, thus indicating their anti-aging activity. Among the four *Ever-roses* varieties, ER011(P) showed the best antioxidant and anti-aging effects, which is attributable to its relatively high content of antioxidant compounds. *Ever-rose* features an attractive appearance and a strong fragrance; additionally, it can be cultivate easily, thus rendering it an excellent choice for garden flowers. It exhibits significant potential as a promising functional cosmetic raw material owing to its excellent antioxidant and anti-aging effects. Our findings can be applied to increase the utilization and market value of *Ever-rose*.

Abbreviations

AFM	Atomic force microscopy
DPPH	2,2-Diphenyl-1-picrylhydrazyl
ECM	Extracellular matrix
HDFs	Human dermal fibroblasts
IRA	Infrared A
ER004(L)	Leaf extracts of ER004
ER011(L)	Leaf extracts of ER011
ER012(L)	Leaf extracts of ER012
ER015(L)	Leaf extracts of ER015
MMPs	Matrix metalloproteinases
PIP	Procollagen type I C-peptide
ER004(P)	Petal extracts of ER004
ER011(P)	Petal extracts of ER011
ER012(P)	Petal extracts of ER012
ER015(P)	Petal extracts of ER015
ROS	Reactive oxygen species
SA-β-gal	Beta-galactosidase
UPHLC-Triple TOF–MS/MS	Ultra-high-performance liquid chromatography triple time-of-flight mass spectrometry/mass spectrometry
UVB	Ultraviolet B
UVP	Ultraviolet P
XOD	Xanthine oxidase

Supplementary Information

The online version contains supplementary material available at https://doi.org/10.1186/s40538-024-00653-2.

Supplementary material 1.

Acknowledgements
Not applicable.

Author contributions
(1) Conception and design of the study—Kyung Sook Kim, Jihui Jang, Jun Bae Lee, Se Jik Han, Polina Belousova, Sangwoo Kwon. (2) Acquisition of data, or analysis and interpretation of data—Se Jik Han, Polina Belousova, Sangwoo Kwon, Hyunjae Kim, Gayeon You, Jihyeon Song, Min Young Lee, Hyejung Mok, Ho Su Ha. (3) Drafting of the article or revising it critically for important intellectual content—Kyung Sook Kim, Hyejung Mok, In Jin Ha, Hyunjae Kim. (4) Final approval of the version to be published—Kyung Sook Kim.

Funding
This study was supported by a grant from Kyung Hee University in 2021 (KHU- 20210133).

Availability of data and materials
The datasets used and/or analyzed during the current study are available from the corresponding author upon reasonable request.

Declarations

Ethics approval and consent to participate
Not applicable.

Consent for publication
Not applicable.

Competing interests
The authors declare no competing interests.

Author details
[1]Department of Biomedical Engineering, Graduate School, Kyung Hee University, Seoul 02447, Republic of Korea. [2]Department of Biomedical Engineering, College of Medicine, Kyung Hee University, Seoul 02447, Republic of Korea. [3]Department of Innovation, Innovation Lab, Cosmax R&I, Seongnam-si, Gyeonggi-Do, Republic of Korea. [4]Department of New Material Development,

COSMAXBIO, Seongnam-si, Gyeonggi-Do, Republic of Korea. [5]Department of Bioscience and Biotechnology, Konkuk University, Seoul 143-701, Republic of Korea. [6]Department of Plant & Contents, Resort Business Division, Samsung C&T Corporation, Yongin-si, Gyeonggi-Do, Republic of Korea. [7]Korean Medicine Clinical Trial Center (K-CTC), Korean Medicine Hospital, Kyung Hee University, Seoul, Republic of Korea.

Received: 20 March 2024 Accepted: 15 August 2024
Published online: 22 August 2024

References

1. Roh E, Kim JE, Kwon JY, Park JS, Park JS, Ann M. Molecular mechanisms of green tea polyphenols with protective effects against skin photoaging. Crit Rev Food Sci Nutr. 2017;57:1631–7.
2. McCabe MC, Hill RC, Calderone K, Cui Y, Yan Y, Quan T, Fisher GJ, Hansen KC. Alterations in extracellular matrix composition during aging and photoaging of the skin. Matrix Biol Plus. 2020;8:100041.
3. Park G, Baek S, Kim JE, Lim TG, Lee CC, Yang H, Kang YG, Park JS, Augustin M, Mrosek M, Lee CY, Dong Z, Huber R, Lee KW. Flt3 is a target of coumestrol in protecting against UVB-induced skin photoaging. Biochem Pharmacol. 2015;98:473–83.
4. Yeo I, Lee YJ, Song K, Jin HS, Lee JE, Kim D, Lee DW, Kang NJ. Low-molecular weight keratins with anti-skin aging activity produced by anaerobic digestion of poultry feathers with Fervidobacterium islandicum AW-1. J Biotechnol. 2018;271:17–25.
5. Willcox JK, Ash SL, Catignani GL. Antioxidants and prevention of chronic disease. Crit Rev Food Sci Nutr. 2004;44:275–95.
6. Wei RB, Yang Q, Pang YX, Yuan L, Zhang YB, Wang ZY. A Comparative study on antioxidant activity of total phenolic acid and flavonoids from different parts of Blumea balsamifera. Nat Prod Res Dev. 2015;27:1242–7.
7. Phetcharat L, Wongsuphasawat K, Winther K. The effectiveness of a standardized rose hip powder, containing seeds and shells of *Rosa canina*, on cell longevity, skin wrinkles, moisture, and elasticity. Clin Interv Aging. 2015;10:1849–56.
8. Yang H, Shin Y. Antioxidant compounds and activities of edible roses (Rosa hybrida spp.) from different cultivars grown in Korea. Appl Biol Chem. 2017;60(2):129–36.
9. Choi JK, Lee YB, Lee Lee KH, Im HC, Kim YB, Choi EK, Joo SS, Jang SK, Han NS, Kim CH. Extraction conditions for phenolic compounds with antioxidant activities from white rose petals. J Appl Biol Chem. 2015;58(2):117–24.
10. Boskabady MH, Shafei MN, Saberi Z, Amini S. Pharmacological effects of *Rosa Damascena*. Iran J Basic Med Sci. 2011;14(4):295–307.
11. Ghavam M, Afzali A, Manconi M, Gianluigi B, Maria LM. Variability in chemical composition and antimicrobial activity of essential oil of Rosa × damascena Herrm. from mountainous regions of Iran. Chem Biol Technol Agric. 2021;8:22.
12. Gudin S. Rose: genetics and breeding. Plant Breed Rev. 2000;17:159–89.
13. Bown D. The herb society of America New Encyclopedia of herbs and their uses. London: Dorling Kindersley Ltd.; 2001.
14. Grieve M. A modern herbal, vol. 2. New York: Dover Publications Inc; 1971.
15. Schnaubelt K. Advanced aromatherapy. Rochester: Healing Arts Press; 1998.
16. Kumar R, Nair V, Singh S, Gupta YK. In vivo antiarthritic activity of Rosa centifolia L. flower extract. Ayu. 2015;36(3):341–5.
17. Hubert J, Kotland A, Henes B, Poigny S, Wandrey F. Deciphering the phytochemical profile of an Alpine Rose (*Rhododendron ferrugineum* L.) leaf extract for a better understanding of its senolytic and skin-rejuvenation effects. Cosmetics. 2022;9:37.
18. Zhang C, Bruins ME, Yang ZQ, Liu ST, Rao PF. A new formula to calculate activity of superoxide dismutase in indirect assays. Anal Biochem. 2016;503:65–7.
19. Liu X, Wu D, Liu J, Li G, Zhang Z, Chen C, Zhang L, Li J. Characterization of xanthine oxidase inhibitory activities of phenols from pickled radish with molecular simulation. Food Chem X. 2022;30:100343.
20. Olamide EA, Funsho OO, Tan NH, Zeng GZ. In vitro antioxidant activity, total phenolic and flavonoid contents of ethanol extract of stem and leaf of Grewia carpinifolia. Beni-Suef Univ J Basic Appl Sci. 2017;6(1):10–4.
21. Kim JY, Kim SJ, You G, Choi ES, Lee JH, Mok H. Protective effects of titanium dioxide-based emulsion after short-term and long-term infrared-A ray irradiation on skin cells. Biotechnol Bioproc E. 2021;26:595–605.
22. Kontomaris SV, Stylianou A, Chliveros G, Malamou A. Determining spatial variability of elastic properties for biological samples using AFM. Micromachines (Basel). 2023;14(1):82.
23. Neeraj K, Pamita B, Bikram S, Shamsher SB. Antioxidant activity and ultra-performance LC-electrospray ionization-quadrupole time-of-flight mass spectrometry for phenolics-based fingerprinting of Rose species: Rosa damascene, Rosa bourboniana and Rosa brunonii. Food Chem Toxicol. 2009;47:361–7.
24. Hvattum E. Determination of phenolic compounds in rose hip (Rosa canina) using liquid chromatography coupled to electrospray ionisation tandem mass spectrometry and diode-array detection. Rapid Commun Mass Spectrom. 2002;16(7):655–62.
25. Borut P, Dahmane R. Free radicals and extrinsic skin aging. Dermatol Res Pract. Hindawi Limited,2012:135206.
26. Han JH, Moon HK, Chung SK, Kang WW. Comparison of physiological activities of radish bud (Raphanus sativus L.) according to extraction solvent and sprouting period. J Korean Soc Food Sci Nutr. 2015;44:549–56.
27. Kim TY, Jeon TW, Yeo SH, Kim SB, Kim JS, Kwak JS. Antimicrobial, antioxidant and SOD-like activity effect of Jubak extracts. Korean J Food Nutr. 2015;23:299–305.
28. Masaki H. Role of antioxidants in the skin: anti-aging effects. J Dermatol Sci. 2010;58(2):85–90.
29. Rahman MM, Islam MB, Khurshid BM, Alam AH. In vitro antioxidant and free radical scavenging activity of different parts of *Tabebuia pallida* growing in Bangladesh. BMC Res Notes. 2015;8:621.
30. Zeng H, Yang R, Lei L, Wang Y. Total flavonoid content, the antioxidant capacity, fingerprinting and quantitative analysis of fupenzi (*Rubus chingii* Hu.). Chin Med. 2015;6:204–13.
31. Veraa N, Zampinib C, Islab MI, Bardóna A. Bardóna antioxidant and XOD inhibitory coumarins from *Pterocaulon polystachyum* DC. Nat Prod Commun. 2007;2(5). https://doi.org/10.1177/1934578X0700200508.
32. Pittayapruek P, Meephansan J, Prapapan O, Komine M, Ohtsuki M. Role of matrix metalloproteinases in photoaging and photocarcinogenesis. Int J Mol Sci. 2016;17(6):868.
33. Kim DJ, Iwasaki A, Chien AL, Kang S. UVB-mediated DNA damage induces matrix metalloproteinases to promote photoaging in an AhR- and SP1-dependent manner. JCI Insight. 2022;7(9):e156344.
34. Kim J, Lee CW, Kim EK, Lee SJ, Park NH, Kim HS, Kim HK, Char K, Jang YP, Kim JW. Inhibition effect of Gynura procumbens extract on UVB-induced matrix-metalloproteinase expression in human dermal fibroblasts. J Ethnopharmacol. 2011;137:427–33.
35. Saunders WB, Bayless KJ, Davis GE. MMP-1 activation by serine proteases and MMP-10 induces human capillary tubular network collapse and regression in 3D collagen matrices. J Cell Sci. 2005;118(Pt 10):2325–40.
36. Argyropoulos AJ, Robichaud P, Balimunkwe RM, Fisher GJ, Hammerberg C, Yan Y, Quan T. Alterations of dermal connective tissue collagen in diabetes: molecular basis of aged-appearing skin. PLoS ONE. 2016;11:e0153806.
37. Park MJ, Bae YS. Fermented Acanthopanax koreanum root extract reduces UVB- and H_2O_2-induced senescence in human skin fibroblast cells. J Microbiol Biotechnol. 2016;26:1224–33.
38. Yaar M, Gilchrest BA. Photoageing: mechanism, prevention and therapy. Br J Dermatol. 2007;157:874–87.
39. Yang J, Song J, Kim SJ, You G, Lee JB, Mok H. Chronic infrared-A irradiation-induced photoaging of human dermal fibroblasts from different donors at physiological temperature. Photodermatol Photo. 2022;38:571–81.
40. Guo C, Sun L, Chen X, Zhang D. Oxidative stress, mitochondrial damage and neurodegenerative diseases. Neural Regen Res. 2013;8:2003–14.
41. Dupont E, Gomez J, Bilodeau D. Beyond UV radiation: a skin under challenge. Int J Cosmet Sci. 2013;35:224–32.
42. Maureen RD, Diana AB. Activation of apoptosis signalling pathways by reactive oxygen species. Biochem Biophys Acta. 2016;863:2977–92.
43. Han R, Chen JA. Modified Sneddon model for the contact between conical indenters and spherical samples. J Mater Res. 2021;36:1762–71.

44. Kwon S, Kim KS. Qualitative analysis of contribution of intracellular skeletal changes to cellular elasticity. Cell Mol Life Sci. 2020;77(7):1345–55.
45. Ishikawa K, Kataoka M, Yanamoto T, Nakabayashi M, Watanabe M, Ishihara S, Yamaguchi S. Crystal structure of β-galactosidase from *Bacillus circulans* ATCC 31382 (BgaD) and the construction of the thermophilic mutants. FEBS J. 2015;282(13):2540–52.
46. Dimri GP, Lee X, Basile G, Acosta M, Scott G, Roskelley C, Medrano EE, Linskens M, Rubelj I, Pereira-Smith O. A biomarker that identifies senescent human cells in culture and in aging skin in vivo. Proc Natl Acad Sci USA. 1995;92(20):9363–7.
47. Lee BY, Han JA, Im JS, Morrone A, Johung K, Goodwin EC, Kleijer WJ, DiMaio D, Hwang ES. Senescence-associated beta-galactosidase is lysosomal beta-galactosidase. Aging Cell. 2006;5(2):187–95.
48. Kong R, Cui Y, Fisher GJ, Wang X, Chen Y, Schneider LM, Majmudar G. A comparative study of the effects of retinol and retinoic acid on histological, molecular, and clinical properties of human skin. J Cosmet Dermatol. 2016;15(1):49–57.
49. Turrens JF. Mitochondrial formation of reactive oxygen species. J Physiol. 2003;552(Pt2):335–44.
50. Hajam YA, Rani R, Ganie SY, Sheikh TA, Javaid D, Qadri SS, Pramodh S, Alsulimani A, Alkhanani MF, Harakeh S, Hussain A, Haque S, Reshi MS. Oxidative stress in human pathology and aging: molecular mechanisms and perspectives. Cells. 2022;11(3):552.
51. Asale Y, Dessalegn E, Assefa D, Abdisa M. Phytochemicals and antioxidant activity of different apple cultivars grown in South Ethiopia: case of the wolayta zone. Int J Food Prop. 2021;24(1):354–63.
52. Jung YH, Chae CW, Choi GE, Shin HC, Lim JR, Chang HS, Park J, Cho JH, Park MR, Lee HJ, Han HJ. Cyanidin 3-*O*-arabinoside suppresses DHT-induced dermal papilla cell senescence by modulating p38-dependent ER-mitochondria contacts. J Biomed Sci. 2022;29:17.
53. Ren J, Lu Y, Qian Y, Chen B, Wu T, Ji G. Recent progress regarding kaempferol for the treatment of various diseases (Review). Exp Ther Med. 2019;18:2759–76.
54. Anand David AV, Arulmoli R, Parasuraman S. Overviews of biological importance of quercetin: a bioactive flavonoid. Pharmacogn Rev. 2016;10(20):84–9.

Publisher's Note